Published for SISSA by Springer

Received: March 25, 2015
Accepted: May 27, 2015
Published: June 18, 2015

Measurement of the time-dependent CP asymmetries in $B_s^0 \to J/\psi K_S^0$

The LHCb collaboration

E-mail: debkr@nikhef.nl

Abstract: The first measurement of decay-time-dependent CP asymmetries in the decay $B_s^0 \to J/\psi K_S^0$ and an updated measurement of the ratio of branching fractions $\mathcal{B}(B_s^0 \to J/\psi K_S^0)/\mathcal{B}(B^0 \to J/\psi K_S^0)$ are presented. The results are obtained using data corresponding to an integrated luminosity of $3.0\,\text{fb}^{-1}$ of proton-proton collisions recorded with the LHCb detector at centre-of-mass energies of 7 and 8 TeV. The results on the CP asymmetries are

$$\begin{aligned}
\mathcal{A}_{\Delta\Gamma}(B_s^0 \to J/\psi K_S^0) &= \quad 0.49 \pm^{0.77}_{0.65} (\text{stat}) \pm 0.06(\text{syst}) \,, \\
C_{\text{dir}}(B_s^0 \to J/\psi K_S^0) &= -0.28 \pm 0.41(\text{stat}) \pm 0.08(\text{syst}) \,, \\
S_{\text{mix}}(B_s^0 \to J/\psi K_S^0) &= -0.08 \pm 0.40(\text{stat}) \pm 0.08(\text{syst}) \,.
\end{aligned}$$

The ratio $\mathcal{B}(B_s^0 \to J/\psi K_S^0)/\mathcal{B}(B^0 \to J/\psi K_S^0)$ is measured to be

$$0.0431 \pm 0.0017(\text{stat}) \pm 0.0012(\text{syst}) \pm 0.0025(f_s/f_d) \,,$$

where the last uncertainty is due to the knowledge of the B_s^0 and B^0 production fractions.

Keywords: CP violation, Hadron-Hadron Scattering, Branching fraction, B physics, Flavor physics

ArXiv ePrint: 1503.07055

Open Access, Copyright CERN,
for the benefit of the LHCb Collaboration.
Article funded by SCOAP^3.

doi:10.1007/JHEP06(2015)131

JHEP06(2015)131

Contents

1 Introduction 1

2 Detector and simulation 4

3 Event selection 4
- 3.1 Initial selection 4
- 3.2 Multivariate selection 5

4 Flavour tagging 6

5 Likelihood fit 8
- 5.1 Mass PDF 8
- 5.2 Decay time PDF 8
- 5.3 Likelihood fit 9
- 5.4 Fit results 10

6 Systematic uncertainties 11

7 Branching ratio measurement 12

8 Conclusion 13

The LHCb collaboration 17

JHEP06(2015)131

1 Introduction

In decays of neutral B mesons (where B stands for a B^0 or B_s^0 meson) to a final state accessible to both B and $\overline{B}$, the interference between the direct decay and the decay via oscillation leads to decay-time-dependent CP violation. Measurements of time-dependent CP asymmetries provide valuable tests of the flavour sector of the Standard Model (SM) and offer opportunities to search for signs of non-SM physics. A measurement of this asymmetry in the $B^0 \to J/\psi\, K^0_{\rm S}$ decay mode allows for a determination of the effective CP phase [1–3]

$$\phi_d^{\rm eff}(B^0 \to J/\psi\, K^0_{\rm S}) \equiv \phi_d + \Delta\phi_d\,, \tag{1.1}$$

where ϕ_d is the relative phase of the B^0–$\overline{B}^0$ mixing amplitude and the tree-level decay process, and $\Delta\phi_d$ is a shift induced by the so-called penguin topologies, which are illustrated in figure 1. In the Standard Model, ϕ_d is equal to 2β [4], where $\beta \equiv \arg(-V_{cd}V_{cb}^*/V_{td}V_{tb}^*)$ is one of the angles of the unitarity triangle in the Cabibbo-Kobayashi-Maskawa (CKM) quark mixing matrix [5, 6]. The latest average of the Belle and BaBar measurements

reads $\sin\phi_d^{\rm eff} = 0.665 \pm 0.020$ [7], while the recently updated analysis from LHCb reports $\sin\phi_d^{\rm eff} = 0.729 \pm 0.035({\rm stat}) \pm 0.022({\rm syst})$ [8].

Forthcoming data from the LHC and KEK e^+e^- super B factory will lead to an unprecedented precision on the phase $\phi_d^{\rm eff}$. To translate this into an equally precise determination of the CKM phase β, it is essential to take into account the doubly Cabibbo-suppressed contributions from the penguin topologies, which lead to a value for $\Delta\phi_d$ that might be as large as $\mathcal{O}(1^\circ)$ [1, 3]. By relying on approximate flavour symmetries, information on $\Delta\phi_d$ can be obtained from measurements of CP asymmetries in decays where the penguin topologies are enhanced. The $B_s^0 \to J/\psi\, K_{\rm S}^0$ mode is the most promising candidate for this task [2, 3, 9].

Assuming no CP violation in mixing [7], the time-dependent CP asymmetry in $B_s^0 \to J/\psi\, K_{\rm S}^0$ takes the form

$$a_{CP}(t) \equiv \frac{\Gamma(\overline{B}_s^0(t) \to J/\psi\, K_{\rm S}^0) - \Gamma(B_s^0(t) \to J/\psi\, K_{\rm S}^0)}{\Gamma(\overline{B}_s^0(t) \to J/\psi\, K_{\rm S}^0) + \Gamma(B_s^0(t) \to J/\psi\, K_{\rm S}^0)}\,, \tag{1.2}$$

$$= \frac{S_{\rm mix}\sin(\Delta m_s\, t) - C_{\rm dir}\cos(\Delta m_s\, t)}{\cosh(\Delta\Gamma_s\, t/2) + \mathcal{A}_{\Delta\Gamma}\sinh(\Delta\Gamma_s\, t/2)}\,, \tag{1.3}$$

where $\Gamma(B_s^0(t) \to J/\psi\, K_{\rm S}^0)$ represents the time-dependent decay rate of the B_s^0 meson into the $J/\psi\, K_{\rm S}^0$ final state, and $\Delta m_s \equiv m_{\rm H} - m_{\rm L}$ and $\Delta\Gamma_s \equiv \Gamma_{\rm L} - \Gamma_{\rm H}$ are, respectively, the mass and decay width difference between the heavy and light eigenstates of the B_s^0 meson system. The $B_s^0 \to J/\psi\, K_{\rm S}^0$ CP observables are defined through the parameter

$$\lambda_{J/\psi\, K_{\rm S}^0} \equiv -e^{i\phi_s}\,\frac{A(\overline{B}_s^0 \to J/\psi\, K_{\rm S}^0)}{A(B_s^0 \to J/\psi\, K_{\rm S}^0)} \tag{1.4}$$

in terms of the complex phase ϕ_s associated with the B_s^0–$\overline{B}_s^0$ mixing process and the ratio of time-independent transition amplitudes as

$$\mathcal{A}_{\Delta\Gamma} \equiv -\frac{2\,\mathcal{R}e[\lambda_{J/\psi\, K_{\rm S}^0}]}{1+|\lambda_{J/\psi\, K_{\rm S}^0}|^2}\,, \qquad C_{\rm dir} \equiv \frac{1-|\lambda_{J/\psi\, K_{\rm S}^0}|^2}{1+|\lambda_{J/\psi\, K_{\rm S}^0}|^2}\,, \qquad S_{\rm mix} \equiv \frac{2\,\mathcal{I}m[\lambda_{J/\psi\, K_{\rm S}^0}]}{1+|\lambda_{J/\psi\, K_{\rm S}^0}|^2}\,, \tag{1.5}$$

where $C_{\rm dir}$ and $S_{\rm mix}$ represent direct and mixing-induced CP violation, respectively. In the Standard Model $\phi_s^{\rm SM} \equiv 2\arg(-V_{ts}V_{tb}^*)$. A recent analysis [3] predicts

$$\begin{aligned} \mathcal{A}_{\Delta\Gamma}\left(B_s^0 \to J/\psi\, K_{\rm S}^0\right) &= 0.957 \pm 0.061\,, \\ C_{\rm dir}\left(B_s^0 \to J/\psi\, K_{\rm S}^0\right) &= 0.003 \pm 0.021\,, \\ S_{\rm mix}\left(B_s^0 \to J/\psi\, K_{\rm S}^0\right) &= 0.29 \ \ \pm 0.20 \ \ . \end{aligned} \tag{1.6}$$

Similar expression for eqs. (1.3) and (1.5) are obtained for the $B^0 \to J/\psi\, K_{\rm S}^0$ decay by replacing $s \leftrightarrow d$. The observable $\mathcal{A}_{\Delta\Gamma}$ is not applicable in the measurement of $B^0 \to J/\psi\, K_{\rm S}^0$ because it is assumed that $\Delta\Gamma_d = 0$ [7].

This paper presents the first measurement of the time-dependent CP asymmetries in $B_s^0 \to J/\psi\, K_{\rm S}^0$ decays, as well as an updated measurement of the ratio of time-integrated branching fractions $\mathcal{B}(B_s^0 \to J/\psi\, K_{\rm S}^0)/\mathcal{B}(B^0 \to J/\psi\, K_{\rm S}^0)$. This ratio was first measured by

JHEP06(2015)131

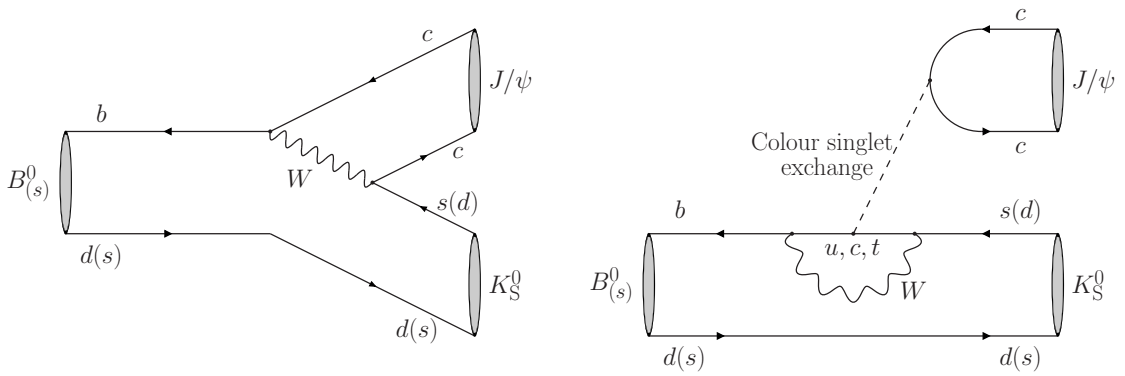

Figure 1. Decay topologies contributing to the $B^0_{(s)} \to J/\psi K^0_S$ channel: (left) tree diagram and (right) penguin diagram.

the CDF collaboration [10], while the previously most precise measurement was reported by LHCb in ref. [11]. The analysis is performed with a data sample corresponding to an integrated luminosity of 3.0 fb^{-1} of proton-proton (pp) collisions, recorded by the LHCb experiment at centre-of-mass energies of 7 TeV and 8 TeV in 2011 and 2012, respectively.

The analysis proceeds in two steps. The first step, described in detail in section 3, consists of a multivariate selection of $B \to J/\psi K^0_S$ candidates. In the second step a maximum likelihood fit is performed to the selected data. The fit model includes a prominent $B^0 \to J/\psi K^0_S$ component, which is used to improve the modelling of the $B^0_s \to J/\psi K^0_S$ signal. In addition, the measurement of CP asymmetries associated with $B^0 \to J/\psi K^0_S$ decays offers a validation of the likelihood method's implementation. However, the stringent event selection necessary to isolate the $B^0_s \to J/\psi K^0_S$ candidates limits the precision on these two CP observables. Dedicated and more precise measurements of the $B^0 \to J/\psi K^0_S$ CP observables are therefore the subject of a separate publication [8].

For a time-dependent measurement of CP violation it is essential to determine the initial flavour of the B candidate, i.e. whether it contained a b or a $\bar{b}$ quark at production. The method to achieve this is called *flavour tagging*, and is discussed in section 4. The tagging information is combined with a description of the B mass and decay time distributions when performing the maximum likelihood fit, which is described in section 5. The three CP observables describing the $B^0_s \to J/\psi K^0_S$ decays and two CP observables describing the $B^0 \to J/\psi K^0_S$ decays are obtained directly from the fit. The ratio of branching fractions [12] is derived from the ratio R of fitted $B^0_s \to J/\psi K^0_S$ to $B^0 \to J/\psi K^0_S$ event yields as

$$\frac{\mathcal{B}(B^0_s \to J/\psi K^0_S)}{\mathcal{B}(B^0 \to J/\psi K^0_S)} = R \times f_{\rm sel} \times \frac{f_d}{f_s}\,, \tag{1.7}$$

where $f_{\rm sel}$ is a correction factor for differences in selection efficiency between $B^0 \to J/\psi K^0_S$ and $B^0_s \to J/\psi K^0_S$ decays, and $f_s/f_d = 0.259 \pm 0.015$ [13, 14] is the ratio of B^0_s to B^0 meson hadronisation fractions. The study of systematic effects on the ratio R and the CP observables is presented in section 6. The main results for the branching ratio measurement are reported in section 7 and those for the CP observables in section 8.

JHEP06(2015)131

2 Detector and simulation

The LHCb detector [15, 16] is a single-arm forward spectrometer covering the pseudorapidity range $2 < \eta < 5$, designed for the study of particles containing b or c quarks. The detector includes a high-precision tracking system consisting of a silicon-strip vertex detector surrounding the pp interaction region, a large-area silicon-strip detector located upstream of a dipole magnet with a bending power of about 4 Tm, and three stations of silicon-strip detectors and straw drift tubes placed downstream of the magnet. The tracking system provides a measurement of momentum, p, of charged particles with a relative uncertainty that varies from 0.5% at low momentum to 1.0% at 200 GeV/c. The minimum distance of a track to a primary vertex, the impact parameter, is measured with a resolution of $(15 + 29/p_{\rm T})$ µm, where $p_{\rm T}$ is the component of the momentum transverse to the beam, in GeV/c. Different types of charged hadrons are distinguished using information from two ring-imaging Cherenkov detectors. Photons, electrons and hadrons are identified by a calorimeter system consisting of scintillating-pad and preshower detectors, an electromagnetic calorimeter and a hadronic calorimeter. Muons are identified by a system composed of alternating layers of iron and multiwire proportional chambers.

In the simulation, pp collisions are generated using Pythia [17, 18] with a specific LHCb configuration [19]. Decays of hadronic particles are described by EvtGen [20], in which final-state radiation is generated using Photos [21]. The interaction of the generated particles with the detector, and its response, are implemented using the Geant4 toolkit [22, 23] as described in ref. [24].

3 Event selection

Candidate $B \to J/\psi K^0_{\rm S}$ decays are considered in the $J/\psi \to \mu^+\mu^-$ and $K^0_{\rm S} \to \pi^+\pi^-$ final states. The event selection is based on an initial selection, followed by a two-stage multivariate analysis consisting of artificial neural network (NN) classifiers [25].

3.1 Initial selection

The online event selection is performed by a trigger, which consists of a hardware level, based on information from the calorimeter and muon systems, followed by a software level, which applies a full event reconstruction. The hardware trigger selects at least one muon with a transverse momentum $p_{\rm T} > 1.48\,(1.76)$ GeV/c or two muons with $\sqrt{p_{\rm T}(\mu_1)p_{\rm T}(\mu_2)} > 1.3\,(1.6)$ GeV/c in the 7 (8) TeV pp collisions. The software trigger consists of two stages. In the first stage, events are required to have either two oppositely charged muons with combined mass above 2.7 GeV/c^2, or at least one muon or one high-$p_{\rm T}$ charged particle ($p_{\rm T} > 1.8$ GeV/c) with an impact parameter larger than 100 µm with respect to all pp interaction vertices (PVs). In the second stage of the software trigger the tracks of two or more of the final-state particles are required to form a vertex that is significantly displaced from the PVs, and only events containing $J/\psi \to \mu^+\mu^-$ candidates are retained.

In the offline selection, J/ψ candidates are selected by requiring two muon tracks to form a good quality vertex and have an invariant mass in the range $[3030, 3150]$ MeV/c^2.

JHEP06(2015)131

This interval corresponds to about eight times the $\mu^+\mu^-$ mass resolution at the J/ψ mass and covers part of the J/ψ radiative tail.

Decays of $K^0_S \to \pi^+\pi^-$ are reconstructed in two different categories: the first involving K^0_S mesons that decay early enough for the daughter pions to be reconstructed in the vertex detector; and the second containing K^0_S that decay later such that track segments of the pions cannot be formed in the vertex detector. These categories are referred to as *long* and *downstream*, respectively. Long K^0_S candidates have better mass, momentum and vertex resolution than those in the downstream category.

The two pion tracks of the long (downstream) K^0_S candidates are required to form a good quality vertex and their combined invariant mass must be within 35(64) MeV/c^2 of the known K^0_S mass [26]. To remove contamination from $\Lambda \to p\pi^-$ decays, the reconstructed mass of the long (downstream) K^0_S candidates under the assumption that one of its daughter tracks is a proton is required to be more than 6 (10) MeV/c^2 away from the known Λ mass [26]. The K^0_S decay vertex is required to be located downstream of the J/ψ decay vertex, i.e. it is required to have a positive flight distance. This removes approximately 50% of mis-reconstructed $B^0 \to J/\psi\, K^*(892)^0$ background. The remaining $B^0 \to J/\psi\, K^*(892)^0$ background is heavily suppressed by the first stage of the multivariate selection described below.

Candidate B mesons are selected from combinations of J/ψ and K^0_S candidates with mass $m_{J/\psi K^0_S}$ in the range $[5180, 5520]$ MeV/c^2 and a decay time larger than 0.2 ps. The reconstructed mass and decay time are obtained from a kinematic fit [27] that constrains the masses of the $\mu^+\mu^-$ and $\pi^+\pi^-$ pairs to the known J/ψ and K^0_S masses [26], respectively, and constrains the B candidate to originate from the PV. A good quality fit is required and the uncertainty on the B mass estimated by the kinematic fit must not exceed 30 MeV/c^2. In the case that the event has multiple PVs, a clear separation of the J/ψ decay vertex from any of the other PVs in the event is required, and all combinations of B candidates and PVs that pass the selection are considered.

3.2 Multivariate selection

The first stage of the multivariate selection focuses on removing the mis-reconstructed $B^0 \to J/\psi\, K^*(892)^0$ background that survives the requirement on the K^0_S flight distance. It only affects the subsample of candidates for which the K^0_S is reconstructed in the long category. The NN is trained on simulated $B^0 \to J/\psi\, K^0_S$ (signal) and $B^0 \to J/\psi\, K^*(892)^0$ (background) data and only uses information associated with the reconstructed pions and K^0_S candidate. This includes decay time, mass, momentum, impact parameter and particle-identification properties. The requirement on the NN classifier's output is optimised to retain 99% of the original signal candidates in simulation, with a background rejection on simulated $B^0 \to J/\psi\, K^*(892)^0$ candidates of 99.55%. This results in an estimated number of 18 ± 2 $B^0 \to J/\psi\, K^*(892)^0$ candidates in the long K^0_S data sample surviving this stage of the selection. Their yield is further reduced by the second NN classifier, and these candidates are therefore treated as combinatorial background in the remainder of the analysis.

The second stage of the multivariate selection aims at reducing the combinatorial background to isolate the small $B^0_s \to J/\psi\, K^0_S$ signal. In contrast to the first NN, it is trained entirely on data, using the $B^0 \to J/\psi\, K^0_S$ signal as a representative of the signal features of

JHEP06(2015)131

the $B_s^0 \to J/\psi K_S^0$ decay. Candidates for the training sample are those populating the mass ranges $[5180, 5340]$ MeV/c^2 and $[5390, 5520]$ MeV/c^2, avoiding the B_s^0 signal region. The signal and background weights for the training of the second NN are determined using the *sPlot* technique [28] and obtained by performing an unbinned maximum likelihood fit to the B mass distribution of the candidates meeting the selection criteria on the first NN classifier's output. The fit function is defined as the sum of a B^0 signal component and a combinatorial background where the parametrisation of the individual components matches that of the likelihood method used for the full *CP* analysis and is described in more detail in section 5.

Due to differences in the distributions of the input variables of the NN, as well as different signal-to-background ratios, the second stage of the multivariate selection is performed separately for the B candidate samples containing long and downstream K_S^0 candidates. The NN classifiers use information on the candidate's kinematic properties, vertex and track quality, impact parameter, particle identification information from the RICH and muon detectors, as well as global event properties like track and PV multiplicities. The variables that are used in the second NN are chosen to avoid correlations with the reconstructed B mass.

Final selection requirements on the second stage NN classifier outputs are chosen to optimise the sensitivity to the B_s^0 signal using $N_S/\sqrt{N_S + N_B}$ as figure of merit, where N_S and N_B are respectively the expected number of signal and background events in a ± 30 MeV/c^2 mass range around the B_s^0 peak. After applying the final requirement on the NN classifier output associated with the long (downstream) K_S^0 sample, the multivariate selection rejects, relative to the initial selection, 99.2% of the background in both samples while keeping 72.9% (58.3%) of the B^0 signal. The lower selection efficiency on the downstream K_S^0 sample is due to the worse signal-to-background ratio after the initial selection, which requires a more stringent requirement on the NN classifier output. The resulting $J/\psi K_S^0$ mass distributions are illustrated in figure 2.

After applying the full selection, the long (downstream) B candidate can still be associated with more than one PV in about 1.5% (0.6%) of the events; in this case, one PVs is chosen at random. Likewise, about 0.24% (0.15%) of the selected events have multiple candidates sharing one or more tracks; in this case, one candidates is chosen at random.

4 Flavour tagging

At the LHC, b quarks are predominantly produced in $b\bar{b}$ pairs. When one of the two quarks hadronises to form the B meson decay of interest ("the signal B"), the other b quark hadronises and decays independently. By exploiting this production mechanism, the signal B's initial flavour is identified by means of two classes of flavour-tagging algorithms. The opposite side (OS) taggers determine the flavour of the non-signal b-hadron [29] while the same side kaon (SSK) tagger exploits the fact that the additional $\overline{s}$ (s) quark produced in the fragmentation of a B_s^0 ($\overline{B}_s^0$) meson often forms a K^+ (K^-) meson [30].

These algorithms provide tag decisions q_{OS} and q_{SSK}, which take the value $+1$ (-1) in case the signal candidate is tagged as a B ($\overline{B}$) meson, and predictions η_{OS} and η_{SSK} for the

JHEP06(2015)131

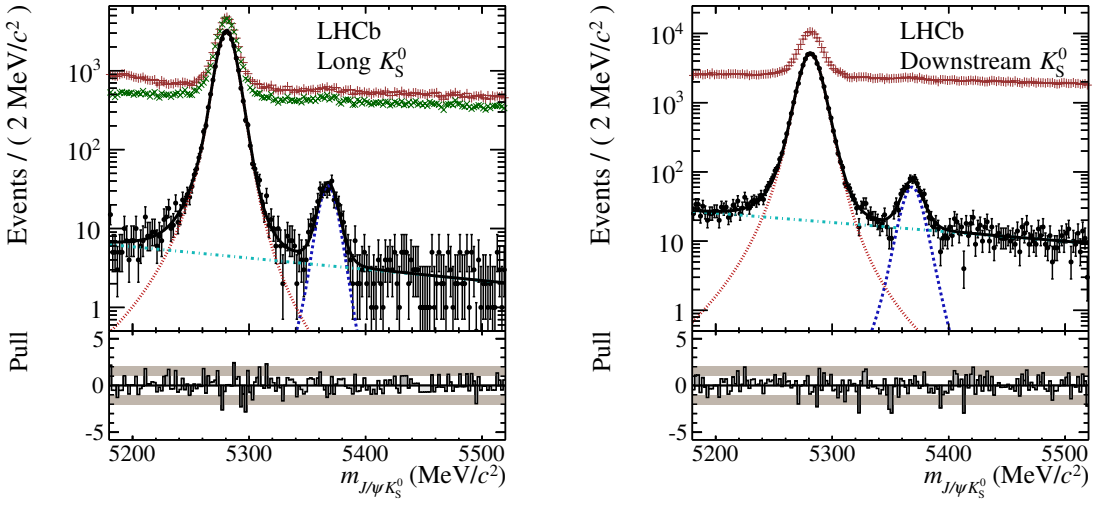

Figure 2. Mass distribution of B candidates at different stages of the event selection for the (left) long K^0_S and (right) downstream K^0_S sample. The data sample after initial selection (red, +), after the first neural net (green, ×) and after the second neural net (black, •) are shown. Overlaid are projections of the fit described in section 5. Shown components are $B^0_s \to J/\psi K^0_S$ (dark blue, dashed), $B^0 \to J/\psi K^0_S$ (red, dotted) and combinatorial background (turquoise, dash-dotted).

probability of the tag to be incorrect. The latter is obtained using neural networks, which in the case of the OS taggers are trained on $B^+ \to J/\psi K^+$ decays, while for the SSK tagger simulated $B^0_s \to D^-_s \pi^+$ events are used.

The mistag probability predicted by the tagging algorithms is calibrated in data to determine the true mistag probability ω, by using control samples of several flavour-specific B mesons decays. This calibration is performed individually for the OS and SSK tagging algorithms; for the latter, different calibration parameters are used to describe the B^0 and B^0_s mesons. For all events with both an OS and SSK tag decision, a combined tag decision and mistag probability is derived as described in ref. [29].

The figure of merit for the optimisation of a tagging algorithm is the effective tagging efficiency, $\varepsilon_{\rm eff} = \varepsilon_{\rm tag}(1-2\omega)^2$ where $\varepsilon_{\rm tag}$ is the fraction of candidates with an assigned tag decision. In the long K^0_S sample for the $B^0_s \to J/\psi K^0_S$ mode, the OS and SSK taggers yield an $\varepsilon_{\rm eff}$ of $(2.93 \pm 0.06)\%$ and $(0.97 \pm 0.12)\%$, respectively, while the sample with both an OS and SSK tagging response gives an $\varepsilon_{\rm eff}$ of $(1.02 \pm 0.10)\%$. In the respective downstream K^0_S sample, the OS and SSK taggers yield an $\varepsilon_{\rm eff}$ of $(2.74 \pm 0.11)\%$ and $(1.45 \pm 0.15)\%$, respectively, while the sample with both an OS and SSK tagging response gives an $\varepsilon_{\rm eff}$ of $(0.48 \pm 0.04)\%$. The combined $\varepsilon_{\rm eff}$ of all three overlapping samples for the $B^0_s \to J/\psi K^0_S$ mode is measured to be $(3.80 \pm 0.18)\%$ and $(4.03 \pm 0.16)\%$ in the long and downstream K^0_S sample, respectively.

In the $B^0 \to J/\psi K^0_S$ mode, the main contribution is provided by the OS taggers, where the combined $\varepsilon_{\rm eff}$ is measured to be $(2.60 \pm 0.05)\%$ and $(2.63 \pm 0.05)\%$ in the long and downstream K^0_S sample, respectively. Although the SSK tagging algorithm is

JHEP06(2015)131

Parameter	Value		Parameter	Value	
Δm_d	0.510 ± 0.003	ps^{-1} [7]	Δm_s	17.757 ± 0.021	ps^{-1} [7]
$\Delta\Gamma_d$	0	ps^{-1}	$\Delta\Gamma_s$	0.081 ± 0.006	ps^{-1} [7]
τ_{B_d}	1.520 ± 0.004	ps [7]	τ_{B_s}	1.509 ± 0.004	ps [7]

Table 1. List of the observables describing the B^0 and B_s^0 systems that are included as Gaussian constraints to the likelihood fit.

specifically designed for B_s^0 mesons, a small, but non-vanishing effective tagging efficiency of $(0.064 \pm 0.009)\%$ and $(0.098 \pm 0.013)\%$ in the long and downstream K_S^0 sample, respectively, is also found for B^0 mesons if the tag decision is reversed. This effect originates from same-side protons mis-identified as kaons, and kaons from the decay of $K^*(892)^0$ mesons produced in correlation with the B^0. Both tagged particles have a charge opposite to those of kaons produced in correlation with the B_s^0, and thus require the SSK tag decision to be inverted. Additionally, mis-identified pions carrying the same charge as the kaons correlated with the B_s^0 dilute the effect described above. The SSK tagging response for B^0 candidates is studied on $B^0 \to J/\psi K^*(892)^0$ candidates using both data and simulated events.

5 Likelihood fit

The $B_s^0 \to J/\psi K_S^0$ *CP* observables are determined from an unbinned maximum likelihood fit. The data is fitted with a probability density function (PDF) defined as the sum of a B^0 signal component, a B_s^0 signal component and a combinatorial background. In total it depends on seven observables. The PDF describes the reconstructed B mass ($m_{J/\psi K_S^0} \in [5180, 5520]$ MeV/c^2), the decay time ($t \in [0.2, 15]$ ps), and tagging responses q_{OS} and q_{SSK}. Additionally, it also depends on the per-candidate decay time uncertainty estimate δ_t and mistag estimates η_{OS} and η_{SSK}. The long and downstream K_S^0 samples are modelled using separate PDFs but fitted simultaneously. The parameters common to both PDFs are the two $B^0 \to J/\psi K_S^0$ and three $B_s^0 \to J/\psi K_S^0$ *CP* observables, as well as the observables describing the B^0 and B_s^0 systems that are listed in table 1.

5.1 Mass PDF

The mass shapes of the $B \to J/\psi K_S^0$ modes in both data and simulation exhibit non-Gaussian tails on both sides of their signal peaks due to final-state radiation, the detector resolution and its dependence on the momenta of the final-state particles. Each signal shape is parametrised by a Hypatia function [31], whose tail parameters are taken from simulation. The B_s^0 component is constrained to have the same shape as the B^0 PDF, but shifted by the B_s^0–B^0 mass difference, which is a free variable in the fit. The mass distribution of the combinatorial background is described by an exponential function.

5.2 Decay time PDF

The decay time distributions of the two signal components, $\mathcal{T}(t, q_{\text{OS}}, q_{\text{SSK}} | \eta_{\text{OS}}, \eta_{\text{SSK}})$, need to be corrected for experimental effects originating from the detector response and the event

JHEP06(2015)131

selection. This is done by convolving them with a resolution model, $\mathcal{R}(t|\delta_t)$, and combining the result with an acceptance function, $\mathcal{E}(t)$, to give the experimentally observed decay-time distribution

$$\left(\int \mathcal{T}(\hat{t}, q_{\rm OS}, q_{\rm SSK} | \eta_{\rm OS}, \eta_{\rm SSK}) \times \mathcal{R}(t - \hat{t} | \delta_t) \, {\rm d}\hat{t} \right) \times \mathcal{E}(t) \, . \tag{5.1}$$

The resolution model has an individual width for each candidate, described by the per-candidate decay-time uncertainty estimate δ_t provided by the kinematic fit introduced in section 3. A finite resolution reduces the amplitude of the oscillating terms in the decay-time distribution by a factor $\mathcal{D} \equiv \exp\left(-\delta_t^2 \Delta m^2/2\right)$ [32, 33], and thereby affects the precision of the time-dependent *CP* observables. This effect is larger for the rapid B_s^0–$\overline{B}{}_s^0$ oscillations than for the B^0–$\overline{B}{}^0$ oscillations. The δ_t estimates are calibrated using a separate sample of prompt J/ψ decays, which are produced directly at the PV and combined with random $K_{\rm S}^0$ candidates. This sample is obtained through the same event selection as described in section 3, except for the requirement on the decay time of the B candidates. The decay time distribution of the prompt J/ψ mesons is modelled by the sum of three Gaussian functions sharing a common mean. For the long (downstream) $K_{\rm S}^0$ sample, this resolution model leads to an average dilution factor of $\langle \mathcal{D} \rangle = 0.73 \pm 0.13$ (0.72 ± 0.04).

The decay time distribution of the two signal components is affected by acceptance effects due to the decay-time bias induced by the trigger selection, the initial selection requirements and, most importantly, the NN classifier outputs. The shapes of the B^0 and B_s^0 acceptances are assumed to be equal and modelled using cubic b-splines [34]. The acceptance function is obtained directly from the data. The $B^0 \to J/\psi K_{\rm S}^0$ decay time distribution is described by a single exponential, assuming $\Delta\Gamma_d = 0$. The lifetime of the B^0, $\tau_{B^0} = 1.520 \pm 0.004$ ps [7], is constrained in the fit using a Gaussian function whose mean is fixed to the known lifetime and whose width accounts for the experimental uncertainty. This allows the acceptance parameters to be directly evaluated in the fit to the data.

The background decay-time distributions are modelled using two exponential functions, describing empirically a short-lived and a long-lived component.

5.3 Likelihood fit

The results are obtained from a simultaneous fit of the long and downstream $K_{\rm S}^0$ samples, using both the OS and SSK tagging information. In addition to the five *CP* observables, the nuisance parameters describing the mass (9 parameters), acceptance (12), background decay time (6) and event yields (18) are floated in the fit. The observables Δm_d, τ_{B^0}, Δm_s, $\tau_{B_s^0}$ and $\Delta\Gamma_s$, parametrising the B^0 and B_s^0 systems, and the effective B production asymmetries $A_{\rm prod}(B^0)$ and $A_{\rm prod}(B_s^0)$ of the long and downstream $K_{\rm S}^0$ samples are constrained using Gaussian functions. The production asymmetries are defined in terms of the B production cross-section $\sigma(B)$ as $A_{\rm prod}(B) \equiv (\sigma(\overline{B}) - \sigma(B))/(\sigma(\overline{B}) + \sigma(B))$. The statistical and systematic uncertainties on the constrained parameters are added in quadrature and treated together; the correlation $\rho(\Gamma_s, \Delta\Gamma_s) = -0.271$ [7] between the decay width and decay width difference of the B_s^0 meson is also included. The effective B production asymmetries, specific to the data sample used in this analysis, are obtained by reweighting the results binned

JHEP06(2015)131

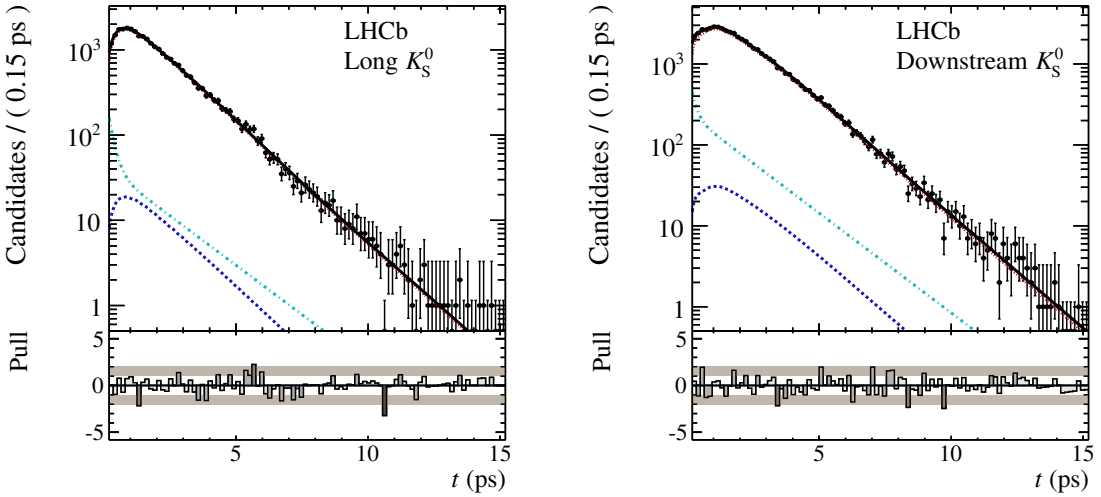

Figure 3. Decay time distribution of B candidates in the (left) long K^0_S and (right) downstream K^0_S sample. The fit projection is shown as solid black line. Shown components are $B^0_s \to J/\psi K^0_S$ (dark blue, dashed), $B^0 \to J/\psi K^0_S$ (red, dotted) and combinatorial background (turquoise, dash-dotted).

Sample	Mode	Value
Long K^0_S	B^0	-0.0117 ± 0.0057 (stat) ± 0.0013 (syst)
Downstream K^0_S	B^0	-0.0095 ± 0.0051 (stat) ± 0.0013 (syst)
Long K^0_S	B^0_s	-0.041 ± 0.032 (stat) ± 0.003 (syst)
Downstream K^0_S	B^0_s	-0.022 ± 0.024 (stat) ± 0.003 (syst)

Table 2. Effective B production asymmetries specific to the data sample used in this analysis.

in B transverse momentum and pseudorapidity given in ref. [35]. The obtained values are listed in table 2.

The likelihood fit is cross-checked using two independent implementations, and is validated with large sets of pseudoexperiments to thoroughly test several aspects of the analysis. These also include the use of stand-alone event generators that produce samples independently of the fit implementations. In addition, the fit model is tested on simulated data, with signal only and with both signal and background components present. The results from the fit to the full data sample are compared to those from various subsamples, and to those obtained from a weighted fit to the $B^0_s \to J/\psi K^0_S$ candidates only. All tests agree with the expectations and no biases in the fit are found.

5.4 Fit results

The results of the $B^0 \to J/\psi K^0_S$ CP asymmetries are

$$C_{\rm dir}\left(B^0 \to J/\psi K^0_S\right) = -0.028 \pm 0.034\,(\text{stat})\,,$$
$$S_{\rm mix}\left(B^0 \to J/\psi K^0_S\right) = 0.719 \pm 0.034\,(\text{stat})\,,$$

JHEP06(2015)131

Yield	Long K^0_S	Downstream K^0_S
$B^0 \to J/\psi K^0_S$	$27\,801 \pm 168$	$51\,351 \pm 231$
$B^0_s \to J/\psi K^0_S$	307 ± 20	601 ± 30
Combinatorial background	658 ± 37	$2\,852 \pm 74$

Table 3. Fitted yields from the unbinned maximum likelihood fit. The uncertainties are statistical only.

where the uncertainties are statistical only. They are compatible with the BaBar [36], Belle [37] and latest LHCb [8] results. The results of the $B^0_s \to J/\psi K^0_S$ *CP* asymmetries are

$$\begin{aligned} \mathcal{A}_{\Delta\Gamma}\left(B^0_s \to J/\psi K^0_S\right) &= 0.49 \pm {}^{0.77}_{0.65}\ (\text{stat})\,, \\ C_{\text{dir}}\left(B^0_s \to J/\psi K^0_S\right) &= -0.28 \pm 0.41\ (\text{stat})\,, \\ S_{\text{mix}}\left(B^0_s \to J/\psi K^0_S\right) &= -0.08 \pm 0.40\ (\text{stat})\,, \end{aligned}$$

where the uncertainties are statistical only, and the observed event yields are summarised in table 3. The fit projections for the mass and decay time distributions are shown in figures 2 and 3, respectively. The statistical correlations between the $B^0_s \to J/\psi K^0_S$ *CP* observables are $\rho(\mathcal{A}_{\Delta\Gamma}, C_{\text{dir}}) = -0.07$, $\rho(\mathcal{A}_{\Delta\Gamma}, S_{\text{mix}}) = -0.01$ and $\rho(C_{\text{dir}}, S_{\text{mix}}) = -0.06$. In addition, there is a $\mathcal{O}(10\%)$ correlation between $\mathcal{A}_{\Delta\Gamma}$ and the average decay width Γ_s and decay width difference $\Delta\Gamma_s$, and a $\mathcal{O}(10\%)$ correlation between S_{mix} and the B^0_s production asymmetries. The confidence intervals for the three $B^0_s \to J/\psi K^0_S$ *CP* asymmetries are also calculated with the Feldman-Cousins method [38, 39], which gives consistent results with the point estimates given above.

6 Systematic uncertainties

A number of systematic uncertainties affecting the determination of the $B^0_s \to J/\psi K^0_S$ *CP* observables and the ratio of event yields R are considered. The main sources of systematic uncertainty are due to assumptions for modelling the different components of the multivariate PDF. These uncertainties are estimated using large sets of simulated pseudoexperiments, in which the shapes and parameters of the individual PDF components are varied. In the generation of the pseudoexperiments, the values of the parameters are fixed to the ones obtained in the fit to the data. For each individual pseudoexperiment, the fitted values of the *CP* observables and event yields are compared between the nominal fit and an alternative fit in which some of the shapes or nuisance parameters are varied. The resulting differences between the fit values form a Gaussian-like distribution. The mean and width of this distribution are added in quadrature and assigned as a systematic uncertainty.

Following this strategy, the systematic uncertainty due to the chosen mass model is evaluated by varying the Hypatia tail parameters within their uncertainties, replacing the signal model with a double Crystal Ball function [40], and replacing the background model with a second-order Chebychev polynomial. The latter variation has the largest impact on the *CP* observables and yield ratio, and is used to assign a systematic uncertainty.

JHEP06(2015)131

Source	$\mathcal{A}_{\Delta\Gamma}$	$C_{\rm dir}$	$S_{\rm mix}$	Long $R \times 10^5$	Downstream $R \times 10^5$
Mass modelling	0.045	0.009	0.009	15.5	17.2
Decay-time resolution	0.038	0.066	0.070	0.6	0.3
Decay-time acceptance	0.022	0.004	0.004	0.6	0.5
Tagging calibration	0.002	0.021	0.023	0.1	0.2
Mass resolution	0.010	0.005	0.006	12.6	8.0
Mass-time correlation	0.003	0.037	0.036	0.2	0.1
Total	0.064	0.079	0.083	20.0	19.0

Table 4. Summary of systematic uncertainties.

The systematic uncertainty associated with the decay time resolution is evaluated by varying the dilution of the resolution model, through changes of the resolution parameters, and by comparing the nominal model with one that includes a scale offset in the calibration functions for the per-candidate decay time uncertainty estimates. The largest impact on the *CP* observables and yield ratio originates from the limited knowledge on the decay time resolution of the long $K^0_{\rm S}$ sample. This forms the dominant systematic uncertainty to the $B^0_s \to J/\psi\, K^0_{\rm S}$ *CP* observables.

Systematic effects due to the modelling of the decay time acceptance mainly affect $\mathcal{A}_{\Delta\Gamma}$, and are evaluated by varying the empirical model for $\mathcal{E}(t)$.

The systematic uncertainty associated with the tagging calibration is obtained by comparing the nominal calibration with the largest and smallest effective tagging efficiency that can be obtained through changes of the calibration parameters within their respective uncertainties.

The mass resolution is assumed to be identical for the B^0 and B^0_s signal modes, but it could depend on the mass of the reconstructed B candidate. This effect is studied by multiplying the width of the B^0_s mass PDF by different scale factors, obtained by comparing B^0 and B^0_s signal shapes in simulation. These variations mainly affect the ratio of event yields.

Finally, a correlation between the reconstructed B mass and decay time resolution is observed in simulated data. The impact of neglecting this correlation in the fit to data is also evaluated with the simulated experiments.

The total systematic uncertainty and its sources are summarised in table 4.

7 Branching ratio measurement

The measured ratio of branching fractions is calculated from the event yields using eq. (1.7). The selection efficiencies and their ratio $f_{\rm sel}$ are evaluated using simulated data. As the simulated data are generated with different values for the lifetime $\tau_{B^0_s}$, decay width difference $\Delta\Gamma_s$ and acceptance parameters compared to those measured in the collision data, correction factors are applied. This leads to a ratio of total selection efficiencies of $f_{\rm sel} = 0.972 \pm 0.029$ for the long $K^0_{\rm S}$ sample and $f_{\rm sel} = 0.987 \pm 0.040$ for the downstream $K^0_{\rm S}$ samples.

JHEP06(2015)131

Combining the results in table 3 with the systematic uncertainties in table 4 yields

$$R\,(\text{long}) = 0.01104 \pm 0.00072\,(\text{stat}) \pm 0.00020\,(\text{syst})\,,$$
$$R\,(\text{downstream}) = 0.01170 \pm 0.00059\,(\text{stat}) \pm 0.00019\,(\text{syst})$$

for the long and downstream K^0_S samples, respectively. A weighted average of the combinations $R \times f_{\text{sel}}$ for the long and downstream K^0_S samples is performed, assuming that they are uncorrelated measurements. The measured ratio of branching fractions is then given by

$$\frac{\mathcal{B}(B^0_s \to J/\psi\, K^0_S)}{\mathcal{B}(B^0 \to J/\psi\, K^0_S)} = 0.0431 \pm 0.0017\,(\text{stat}) \pm 0.0012\,(\text{syst}) \pm 0.0025\,(f_s/f_d)\,.$$

where the third uncertainty is due to the uncertainty in f_s/f_d.

Combining the ratio of branching fractions with the known $B^0 \to J/\psi\, K^0$ branching fraction $\mathcal{B}(B^0 \to J/\psi\, K^0) = (8.97 \pm 0.35) \times 10^{-4}$ [26], which accounts for the difference in production rates for the B^+B^- and $B^0\overline{B}^0$ pairs at the $\Upsilon(4S)$ resonance, i.e. $\Gamma(B^+B^-)/\Gamma(B^0\overline{B}^0) = 1.058 \pm 0.024$ [7], the $B^0_s \to J/\psi\, K^0_S$ branching fraction is

$$\mathcal{B}(B^0_s \to J/\psi\, K^0_S) =$$
$$\left[1.93 \pm 0.08\,(\text{stat}) \pm 0.05\,(\text{syst}) \pm 0.11\,(f_s/f_d) \pm 0.07\,(\mathcal{B}(B^0 \to J/\psi\, K^0)\right] \times 10^{-5}\,,$$

where the last uncertainty comes from the $B^0 \to J/\psi\, K^0$ branching fraction.

8 Conclusion

This paper presents the first measurement of the time-dependent *CP* violation observables in the decay $B^0_s \to J/\psi\, K^0_S$ and an updated measurement of its time-integrated branching fraction. Both measurements are performed using a data set corresponding to an integrated luminosity of 3.0 fb^{-1} of pp collisions recorded by the LHCb detector at centre-of-mass energies of 7 and 8 TeV.

The results on the *CP* observables are

$$\mathcal{A}_{\Delta\Gamma}\left(B^0_s \to J/\psi\, K^0_S\right) = \quad 0.49 \pm {}^{0.77}_{0.65}\ (\text{stat}) \pm 0.06\,(\text{syst})\,,$$
$$C_{\text{dir}}\left(B^0_s \to J/\psi\, K^0_S\right) = -0.28 \pm 0.41\,(\text{stat}) \pm 0.08\,(\text{syst})\,,$$
$$S_{\text{mix}}\left(B^0_s \to J/\psi\, K^0_S\right) = -0.08 \pm 0.40\,(\text{stat}) \pm 0.08\,(\text{syst})\,.$$

The large statistical uncertainties on these results do not allow for a conclusive comparison with the predictions in eq. (1.6) nor do they provide constraints on the shift parameter $\Delta\phi_d$ affecting *CP* measurements in $B^0 \to J/\psi\, K^0_S$.

The ratio of time-integrated branching fractions is measured to be

$$\frac{\mathcal{B}(B^0_s \to J/\psi\, K^0_S)}{\mathcal{B}(B^0 \to J/\psi\, K^0_S)} = 0.0431 \pm 0.0017\,(\text{stat}) \pm 0.0012\,(\text{syst}) \pm 0.0025\,(f_s/f_d)\,.$$

This result is the single most precise measurement of this quantity, and supersedes the previous LHCb measurement [11].

JHEP06(2015)131

Acknowledgments

We express our gratitude to our colleagues in the CERN accelerator departments for the excellent performance of the LHC. We thank the technical and administrative staff at the LHCb institutes. We acknowledge support from CERN and from the national agencies: CAPES, CNPq, FAPERJ and FINEP (Brazil); NSFC (China); CNRS/IN2P3 (France); BMBF, DFG, HGF and MPG (Germany); INFN (Italy); FOM and NWO (The Netherlands); MNiSW and NCN (Poland); MEN/IFA (Romania); MinES and FANO (Russia); MinECo (Spain); SNSF and SER (Switzerland); NASU (Ukraine); STFC (United Kingdom); NSF (USA). The Tier1 computing centres are supported by IN2P3 (France), KIT and BMBF (Germany), INFN (Italy), NWO and SURF (The Netherlands), PIC (Spain), GridPP (United Kingdom). We are indebted to the communities behind the multiple open source software packages on which we depend. We are also thankful for the computing resources and the access to software R&D tools provided by Yandex LLC (Russia). Individual groups or members have received support from EPLANET, Marie Skłodowska-Curie Actions and ERC (European Union), Conseil général de Haute-Savoie, Labex ENIGMASS and OCEVU, Région Auvergne (France), RFBR (Russia), XuntaGal and GENCAT (Spain), Royal Society and Royal Commission for the Exhibition of 1851 (United Kingdom).

Open Access. This article is distributed under the terms of the Creative Commons Attribution License (CC-BY 4.0), which permits any use, distribution and reproduction in any medium, provided the original author(s) and source are credited.

References

[1] S. Faller, M. Jung, R. Fleischer and T. Mannel, *The golden modes $B^0 \to J/\psi K_{S,L}$ in the era of precision flavour physics*, *Phys. Rev.* **D 79** (2009) 014030 [arXiv:0809.0842] [INSPIRE].

[2] K. De Bruyn, R. Fleischer and P. Koppenburg, *Extracting γ and penguin topologies through CP-violation in $B_s^0 \to J/\psi K_S$*, *Eur. Phys. J.* **C 70** (2010) 1025 [arXiv:1010.0089] [INSPIRE].

[3] K. De Bruyn and R. Fleischer, *A roadmap to control penguin effects in $B_d^0 \to J/\psi K_S^0$ and $B_s^0 \to J/\psi\phi$*, *JHEP* **03** (2015) 145 [arXiv:1412.6834] [INSPIRE].

[4] I.I.Y. Bigi and A.I. Sanda, *Notes on the observability of CP-violations in B decays*, *Nucl. Phys.* **B 193** (1981) 85 [INSPIRE].

[5] M. Kobayashi and T. Maskawa, *CP violation in the renormalizable theory of weak interaction*, *Prog. Theor. Phys.* **49** (1973) 652 [INSPIRE].

[6] N. Cabibbo, *Unitary symmetry and leptonic decays*, *Phys. Rev. Lett.* **10** (1963) 531 [INSPIRE].

[7] Heavy Flavor Averaging Group (HFAG) collaboration, Y. Amhis et al., *Averages of b-hadron, c-hadron and τ-lepton properties as of summer 2014*, arXiv:1412.7515 [INSPIRE].

[8] LHCb collaboration, *Measurement of CP violation in $B^0 \to J/\psi K_S^0$ decays*, arXiv:1503.07089 [INSPIRE].

[9] R. Fleischer, *Extracting γ from $B_{(s/d)} \to J/\psi K_S^0$ and $B_{(d/s)} \to D_{(d/s)}^+ D_{(d/s)}^-$*, *Eur. Phys. J.* **C 10** (1999) 299 [hep-ph/9903455] [INSPIRE].

JHEP06(2015)131

[10] CDF collaboration, T. Aaltonen et al., *Observation of $B_s^0 \to J/\psi K^{*0}(892)$ and $B_s^0 \to J/\psi K_S^0$ decays*, *Phys. Rev.* **D 83** (2011) 052012 [arXiv:1102.1961] [INSPIRE].

[11] LHCb collaboration, *Measurement of the effective $B_s^0 \to J/\psi K_S^0$ lifetime*, *Nucl. Phys.* **B 873** (2013) 275 [arXiv:1304.4500] [INSPIRE].

[12] K. De Bruyn et al., *Branching ratio measurements of B_s decays*, *Phys. Rev.* **D 86** (2012) 014027 [arXiv:1204.1735] [INSPIRE].

[13] LHCb collaboration, *Measurement of the fragmentation fraction ratio f_s/f_d and its dependence on B meson kinematics*, *JHEP* **04** (2013) 001 [arXiv:1301.5286] [INSPIRE].

[14] LHCb collaboration, *Updated average f_s/f_d b-hadron production fraction ratio for 7 TeV pp collisions*, LHCb-CONF-2013-011 (2013).

[15] LHCb collaboration, *The LHCb detector at the LHC*, 2008 *JINST* **3** S08005 [INSPIRE].

[16] LHCb collaboration, *LHCb detector performance*, *Int. J. Mod. Phys.* **A 30** (2015) 1530022 [arXiv:1412.6352] [INSPIRE].

[17] T. Sjöstrand, S. Mrenna and P.Z. Skands, *PYTHIA 6.4 physics and manual*, *JHEP* **05** (2006) 026 [hep-ph/0603175] [INSPIRE].

[18] T. Sjöstrand, S. Mrenna and P.Z. Skands, *A brief introduction to PYTHIA 8.1*, *Comput. Phys. Commun.* **178** (2008) 852 [arXiv:0710.3820] [INSPIRE].

[19] LHCb collaboration, *Handling of the generation of primary events in Gauss, the LHCb simulation framework*, *J. Phys. Conf. Ser.* **331** (2011) 032047 [INSPIRE].

[20] D.J. Lange, *The EvtGen particle decay simulation package*, *Nucl. Instrum. Meth.* **A 462** (2001) 152 [INSPIRE].

[21] P. Golonka and Z. Was, *PHOTOS Monte Carlo: A precision tool for QED corrections in Z and W decays*, *Eur. Phys. J.* **C 45** (2006) 97 [hep-ph/0506026] [INSPIRE].

[22] GEANT4 collaboration, J. Allison et al., *Geant4 developments and applications*, *IEEE Trans. Nucl. Sci.* **53** (2006) 270.

[23] GEANT4 collaboration, S. Agostinelli et al., *Geant4: A simulation toolkit*, *Nucl. Instrum. Meth.* **A 506** (2003) 250 [INSPIRE].

[24] LHCb collaboration, *The LHCb simulation application, Gauss: Design, evolution and experience*, *J. Phys. Conf. Ser.* **331** (2011) 032023 [INSPIRE].

[25] M. Feindt, *A neural Bayesian estimator for conditional probability densities*, physics/0402093 [INSPIRE].

[26] PARTICLE DATA GROUP collaboration, K.A. Olive *et al.*, *Review of particle physics*, *Chin. Phys.* **C38** (2014) 090001.

[27] W.D. Hulsbergen, *Decay chain fitting with a Kalman filter*, *Nucl. Instrum. Meth.* **A 552** (2005) 566 [physics/0503191] [INSPIRE].

[28] M. Pivk and F.R. Le Diberder, *SPlot: A statistical tool to unfold data distributions*, *Nucl. Instrum. Meth.* **A 555** (2005) 356 [physics/0402083] [INSPIRE].

[29] LHCb collaboration, *Opposite-side flavour tagging of B mesons at the LHCb experiment*, *Eur. Phys. J.* **C 72** (2012) 2022 [arXiv:1202.4979] [INSPIRE].

[30] LHCb collaboration, *Optimization and calibration of the same-side kaon tagging algorithm using hadronic B_s^0 decays in 2011 data*, LHCb-CONF-2012-033 (2012).

JHEP06(2015)131

[31] D. Martínez Santos and F. Dupertuis, *Mass distributions marginalized over per-event errors*, *Nucl. Instrum. Meth.* **A 764** (2014) 150 [arXiv:1312.5000] [INSPIRE].

[32] H.G. Moser and A. Roussarie, *Mathematical methods for $B^0 - \bar{B}^0$ oscillation analyses*, *Nucl. Instrum. Meth.* **A 384** (1997) 491 [INSPIRE].

[33] LHCb collaboration, *Measurement of CP-violation and the B_s^0 meson decay width difference with $B_s^0 \to J/\psi K^+K^-$ and $B_s^0 \to J/\psi \pi^+\pi^-$ decays*, *Phys. Rev.* **D 87** (2013) 112010 [arXiv:1304.2600] [INSPIRE].

[34] T.M. Karbach, G. Raven and M. Schiller, *Decay time integrals in neutral meson mixing and their efficient evaluation*, arXiv:1407.0748 [INSPIRE].

[35] LHCb collaboration, *Measurement of the $\bar{B}^0 - B^0$ and $\bar{B}_s^0 - B_s^0$ production asymmetries in pp collisions at $\sqrt{s} = 7$ TeV*, *Phys. Lett.* **B 739** (2014) 218 [arXiv:1408.0275] [INSPIRE].

[36] BABAR collaboration, B. Aubert et al., *Measurement of time-dependent CP asymmetry in $B^0 \to c\bar{c}K^{(*)0}$ decays*, *Phys. Rev.* **D 79** (2009) 072009 [arXiv:0902.1708] [INSPIRE].

[37] I. Adachi et al., *Precise measurement of the CP-violation parameter $\sin 2\phi_1$ in $B^0 \to (c\bar{c})K^0$ decays*, *Phys. Rev. Lett.* **108** (2012) 171802 [arXiv:1201.4643] [INSPIRE].

[38] G.J. Feldman and R.D. Cousins, *A Unified approach to the classical statistical analysis of small signals*, *Phys. Rev.* **D 57** (1998) 3873 [physics/9711021] [INSPIRE].

[39] T.M. Karbach, *Feldman-Cousins confidence levels - toy MC method*, arXiv:1109.0714 [INSPIRE].

[40] T. Skwarnicki, *A study of the radiative cascade transitions between the Upsilon-prime and Upsilon resonances*, PhD thesis, Institute of Nuclear Physics, Krakow, 1986, DESY-F31-86-02.

JHEP06(2015)131

The LHCb collaboration

R. Aaij[41], B. Adeva[37], M. Adinolfi[46], A. Affolder[52], Z. Ajaltouni[5], S. Akar[6], J. Albrecht[9], F. Alessio[38], M. Alexander[51], S. Ali[41], G. Alkhazov[30], P. Alvarez Cartelle[53], A.A. Alves Jr[57], S. Amato[2], S. Amerio[22], Y. Amhis[7], L. An[3], L. Anderlini[17,g], J. Anderson[40], M. Andreotti[16,f], J.E. Andrews[58], R.B. Appleby[54], O. Aquines Gutierrez[10], F. Archilli[38], A. Artamonov[35], M. Artuso[59], E. Aslanides[6], G. Auriemma[25,n], M. Baalouch[5], S. Bachmann[11], J.J. Back[48], A. Badalov[36], C. Baesso[60], W. Baldini[16,38], R.J. Barlow[54], C. Barschel[38], S. Barsuk[7], W. Barter[38], V. Batozskaya[28], V. Battista[39], A. Bay[39], L. Beaucourt[4], J. Beddow[51], F. Bedeschi[23], I. Bediaga[1], L.J. Bel[41], I. Belyaev[31], E. Ben-Haim[8], G. Bencivenni[18], S. Benson[38], J. Benton[46], A. Berezhnoy[32], R. Bernet[40], A. Bertolin[22], M.-O. Bettler[38], M. van Beuzekom[41], A. Bien[11], S. Bifani[45], T. Bird[54], A. Bizzeti[17,i], T. Blake[48], F. Blanc[39], J. Blouw[10], S. Blusk[59], V. Bocci[25], A. Bondar[34], N. Bondar[30,38], W. Bonivento[15], S. Borghi[54], A. Borgia[59], M. Borsato[7], T.J.V. Bowcock[52], E. Bowen[40], C. Bozzi[16], S. Braun[11], D. Brett[54], M. Britsch[10], T. Britton[59], J. Brodzicka[54], N.H. Brook[46], A. Bursche[40], J. Buytaert[38], S. Cadeddu[15], R. Calabrese[16,f], M. Calvi[20,k], M. Calvo Gomez[36,p], P. Campana[18], D. Campora Perez[38], L. Capriotti[54], A. Carbone[14,d], G. Carboni[24,l], R. Cardinale[19,j], A. Cardini[15], P. Carniti[20], L. Carson[50], K. Carvalho Akiba[2,38], R. Casanova Mohr[36], G. Casse[52], L. Cassina[20,k], L. Castillo Garcia[38], M. Cattaneo[38], Ch. Cauet[9], G. Cavallero[19], R. Cenci[23,t], M. Charles[8], Ph. Charpentier[38], M. Chefdeville[4], S. Chen[54], S.-F. Cheung[55], N. Chiapolini[40], M. Chrzaszcz[40,26], X. Cid Vidal[38], G. Ciezarek[41], P.E.L. Clarke[50], M. Clemencic[38], H.V. Cliff[47], J. Closier[38], V. Coco[38], J. Cogan[6], E. Cogneras[5], V. Cogoni[15,e], L. Cojocariu[29], G. Collazuol[22], P. Collins[38], A. Comerma-Montells[11], A. Contu[15,38], A. Cook[46], M. Coombes[46], S. Coquereau[8], G. Corti[38], M. Corvo[16,f], I. Counts[56], B. Couturier[38], G.A. Cowan[50], D.C. Craik[48], A.C. Crocombe[48], M. Cruz Torres[60], S. Cunliffe[53], R. Currie[53], C. D'Ambrosio[38], J. Dalseno[46], P.N.Y. David[41], A. Davis[57], K. De Bruyn[41], S. De Capua[54], M. De Cian[11], J.M. De Miranda[1], L. De Paula[2], W. De Silva[57], P. De Simone[18], C.-T. Dean[51], D. Decamp[4], M. Deckenhoff[9], L. Del Buono[8], N. Déléage[4], D. Derkach[55], O. Deschamps[5], F. Dettori[38], B. Dey[40], A. Di Canto[38], F. Di Ruscio[24], H. Dijkstra[38], S. Donleavy[52], F. Dordei[11], M. Dorigo[39], A. Dosil Suárez[37], D. Dossett[48], A. Dovbnya[43], K. Dreimanis[52], G. Dujany[54], F. Dupertuis[39], P. Durante[38], R. Dzhelyadin[35], A. Dziurda[26], A. Dzyuba[30], S. Easo[49,38], U. Egede[53], V. Egorychev[31], S. Eidelman[34], S. Eisenhardt[50], U. Eitschberger[9], R. Ekelhof[9], L. Eklund[51], I. El Rifai[5], Ch. Elsasser[40], S. Ely[59], S. Esen[11], H.M. Evans[47], T. Evans[55], A. Falabella[14], C. Färber[11], C. Farinelli[41], N. Farley[45], S. Farry[52], R. Fay[52], D. Ferguson[50], V. Fernandez Albor[37], F. Ferreira Rodrigues[1], M. Ferro-Luzzi[38], S. Filippov[33], M. Fiore[16,38,f], M. Fiorini[16,f], M. Firlej[27], C. Fitzpatrick[39], T. Fiutowski[27], P. Fol[53], M. Fontana[10], F. Fontanelli[19,j], R. Forty[38], O. Francisco[2], M. Frank[38], C. Frei[38], M. Frosini[17], J. Fu[21,38], E. Furfaro[24,l], A. Gallas Torreira[37], D. Galli[14,d], S. Gallorini[22,38], S. Gambetta[19,j], M. Gandelman[2], P. Gandini[55], Y. Gao[3], J. García Pardiñas[37], J. Garofoli[59], J. Garra Tico[47], L. Garrido[36], D. Gascon[36], C. Gaspar[38], U. Gastaldi[16], R. Gauld[55], L. Gavardi[9], G. Gazzoni[5], A. Geraci[21,v], E. Gersabeck[11], M. Gersabeck[54], T. Gershon[48], Ph. Ghez[4], A. Gianelle[22], S. Gianì[39], V. Gibson[47], L. Giubega[29], V.V. Gligorov[38], C. Göbel[60], D. Golubkov[31], A. Golutvin[53,31,38], A. Gomes[1,a], C. Gotti[20,k], M. Grabalosa Gándara[5], R. Graciani Diaz[36], L.A. Granado Cardoso[38], E. Graugés[36], E. Graverini[40], G. Graziani[17], A. Grecu[29], E. Greening[55], S. Gregson[47], P. Griffith[45], L. Grillo[11], O. Grünberg[63], E. Gushchin[33], Yu. Guz[35,38], T. Gys[38], C. Hadjivasiliou[59], G. Haefeli[39], C. Haen[38], S.C. Haines[47], S. Hall[53], B. Hamilton[58], T. Hampson[46], X. Han[11], S. Hansmann-Menzemer[11], N. Harnew[55], S.T. Harnew[46], J. Harrison[54], J. He[38], T. Head[39], V. Heijne[41], K. Hennessy[52], P. Henrard[5], L. Henry[8], J.A. Hernando Morata[37], E. van Herwijnen[38], M. Heß[63], A. Hicheur[2], D. Hill[55], M. Hoballah[5], C. Hombach[54], W. Hulsbergen[41], T. Humair[53], N. Hussain[55],

JHEP06(2015)131

D. Hutchcroft[52], D. Hynds[51], M. Idzik[27], P. Ilten[56], R. Jacobsson[38], A. Jaeger[11], J. Jalocha[55], E. Jans[41], A. Jawahery[58], F. Jing[3], M. John[55], D. Johnson[38], C.R. Jones[47], C. Joram[38], B. Jost[38], N. Jurik[59], S. Kandybei[43], W. Kanso[6], M. Karacson[38], T.M. Karbach[38], S. Karodia[51], M. Kelsey[59], I.R. Kenyon[45], M. Kenzie[38], T. Ketel[42], B. Khanji[20,38,k], C. Khurewathanakul[39], S. Klaver[54], K. Klimaszewski[28], O. Kochebina[7], M. Kolpin[11], I. Komarov[39], R.F. Koopman[42], P. Koppenburg[41,38], M. Korolev[32], L. Kravchuk[33], K. Kreplin[11], M. Kreps[48], G. Krocker[11], P. Krokovny[34], F. Kruse[9], W. Kucewicz[26,o], M. Kucharczyk[26], V. Kudryavtsev[34], K. Kurek[28], T. Kvaratskheliya[31], V.N. La Thi[39], D. Lacarrere[38], G. Lafferty[54], A. Lai[15], D. Lambert[50], R.W. Lambert[42], G. Lanfranchi[18], C. Langenbruch[48], B. Langhans[38], T. Latham[48], C. Lazzeroni[45], R. Le Gac[6], J. van Leerdam[41], J.-P. Lees[4], R. Lefèvre[5], A. Leflat[32], J. Lefrançois[7], O. Leroy[6], T. Lesiak[26], B. Leverington[11], Y. Li[7], T. Likhomanenko[64], M. Liles[52], R. Lindner[38], C. Linn[38], F. Lionetto[40], B. Liu[15], S. Lohn[38], I. Longstaff[51], J.H. Lopes[2], P. Lowdon[40], D. Lucchesi[22,r], H. Luo[50], A. Lupato[22], E. Luppi[16,f], O. Lupton[55], F. Machefert[7], I.V. Machikhiliyan[31], F. Maciuc[29], O. Maev[30], S. Malde[55], A. Malinin[64], G. Manca[15,e], G. Mancinelli[6], P. Manning[59], A. Mapelli[38], J. Maratas[5], J.F. Marchand[4], U. Marconi[14], C. Marin Benito[36], P. Marino[23,38,t], R. Märki[39], J. Marks[11], G. Martellotti[25], M. Martinelli[39], D. Martinez Santos[42], F. Martinez Vidal[66], D. Martins Tostes[2], A. Massafferri[1], R. Matev[38], Z. Mathe[38], C. Matteuzzi[20], A. Mauri[40], B. Maurin[39], A. Mazurov[45], M. McCann[53], J. McCarthy[45], A. McNab[54], R. McNulty[12], B. McSkelly[52], B. Meadows[57], F. Meier[9], M. Meissner[11], M. Merk[41], D.A. Milanes[62], M.-N. Minard[4], J. Molina Rodriguez[60], S. Monteil[5], M. Morandin[22], P. Morawski[27], A. Mordà[6], M.J. Morello[23,t], J. Moron[27], A.-B. Morris[50], R. Mountain[59], F. Muheim[50], K. Müller[40], M. Mussini[14], B. Muster[39], P. Naik[46], T. Nakada[39], R. Nandakumar[49], I. Nasteva[2], M. Needham[50], N. Neri[21], S. Neubert[11], N. Neufeld[38], M. Neuner[11], A.D. Nguyen[39], T.D. Nguyen[39], C. Nguyen-Mau[39,q], V. Niess[5], R. Niet[9], N. Nikitin[32], T. Nikodem[11], A. Novoselov[35], D.P. O'Hanlon[48], A. Oblakowska-Mucha[27], V. Obraztsov[35], S. Ogilvy[51], O. Okhrimenko[44], R. Oldeman[15,e], C.J.G. Onderwater[67], B. Osorio Rodrigues[1], J.M. Otalora Goicochea[2], A. Otto[38], P. Owen[53], A. Oyanguren[66], A. Palano[13,c], F. Palombo[21,u], M. Palutan[18], J. Panman[38], A. Papanestis[49], M. Pappagallo[51], L.L. Pappalardo[16,f], C. Parkes[54], G. Passaleva[17], G.D. Patel[52], M. Patel[53], C. Patrignani[19,j], A. Pearce[54,49], A. Pellegrino[41], G. Penso[25,m], M. Pepe Altarelli[38], S. Perazzini[14,d], P. Perret[5], L. Pescatore[45], K. Petridis[46], A. Petrolini[19,j], E. Picatoste Olloqui[36], B. Pietrzyk[4], T. Pilař[48], D. Pinci[25], A. Pistone[19], S. Playfer[50], M. Plo Casasus[37], T. Poikela[38], F. Polci[8], A. Poluektov[48,34], I. Polyakov[31], E. Polycarpo[2], A. Popov[35], D. Popov[10], B. Popovici[29], C. Potterat[2], E. Price[46], J.D. Price[52], J. Prisciandaro[39], A. Pritchard[52], C. Prouve[46], V. Pugatch[44], A. Puig Navarro[39], G. Punzi[23,s], W. Qian[4], R. Quagliani[7,46], B. Rachwal[26], J.H. Rademacker[46], B. Rakotomiaramanana[39], M. Rama[23], M.S. Rangel[2], I. Raniuk[43], N. Rauschmayr[38], G. Raven[42], F. Redi[53], S. Reichert[54], M.M. Reid[48], A.C. dos Reis[1], S. Ricciardi[49], S. Richards[46], M. Rihl[38], K. Rinnert[52], V. Rives Molina[36], P. Robbe[7,38], A.B. Rodrigues[1], E. Rodrigues[54], J.A. Rodriguez Lopez[62], P. Rodriguez Perez[54], S. Roiser[38], V. Romanovsky[35], A. Romero Vidal[37], M. Rotondo[22], J. Rouvinet[39], T. Ruf[38], H. Ruiz[36], P. Ruiz Valls[66], J.J. Saborido Silva[37], N. Sagidova[30], P. Sail[51], B. Saitta[15,e], V. Salustino Guimaraes[2], C. Sanchez Mayordomo[66], B. Sanmartin Sedes[37], R. Santacesaria[25], C. Santamarina Rios[37], E. Santovetti[24,l], A. Sarti[18,m], C. Satriano[25,n], A. Satta[24], D.M. Saunders[46], D. Savrina[31,32], M. Schiller[38], H. Schindler[38], M. Schlupp[9], M. Schmelling[10], B. Schmidt[38], O. Schneider[39], A. Schopper[38], M.-H. Schune[7], R. Schwemmer[38], B. Sciascia[18], A. Sciubba[25,m], A. Semennikov[31], I. Sepp[53], N. Serra[40], J. Serrano[6], L. Sestini[22], P. Seyfert[11], M. Shapkin[35], I. Shapoval[16,43,f], Y. Shcheglov[30], T. Shears[52], L. Shekhtman[34], V. Shevchenko[64], A. Shires[9], R. Silva Coutinho[48], G. Simi[22], M. Sirendi[47], N. Skidmore[46], I. Skillicorn[51], T. Skwarnicki[59], N.A. Smith[52], E. Smith[55,49], E. Smith[53], J. Smith[47], M. Smith[54], H. Snoek[41], M.D. Sokoloff[57,38], F.J.P. Soler[51], F. Soomro[39], D. Souza[46],

JHEP06(2015)131

B. Souza De Paula[2], B. Spaan[9], P. Spradlin[51], S. Sridharan[38], F. Stagni[38], M. Stahl[11], S. Stahl[38], O. Steinkamp[40], O. Stenyakin[35], F. Sterpka[59], S. Stevenson[55], S. Stoica[29], S. Stone[59], B. Storaci[40], S. Stracka[23,t], M. Straticiuc[29], U. Straumann[40], R. Stroili[22], L. Sun[57], W. Sutcliffe[53], K. Swientek[27], S. Swientek[9], V. Syropoulos[42], M. Szczekowski[28], P. Szczypka[39,38], T. Szumlak[27], S. T'Jampens[4], M. Teklishyn[7], G. Tellarini[16,f], F. Teubert[38], C. Thomas[55], E. Thomas[38], J. van Tilburg[41], V. Tisserand[4], M. Tobin[39], J. Todd[57], S. Tolk[42], L. Tomassetti[16,f], D. Tonelli[38], S. Topp-Joergensen[55], N. Torr[55], E. Tournefier[4], S. Tourneur[39], K. Trabelsi[39], M.T. Tran[39], M. Tresch[40], A. Trisovic[38], A. Tsaregorodtsev[6], P. Tsopelas[41], N. Tuning[41,38], M. Ubeda Garcia[38], A. Ukleja[28], A. Ustyuzhanin[65], U. Uwer[11], C. Vacca[15,e], V. Vagnoni[14], G. Valenti[14], A. Vallier[7], R. Vazquez Gomez[18], P. Vazquez Regueiro[37], C. Vázquez Sierra[37], S. Vecchi[16], J.J. Velthuis[46], M. Veltri[17,h], G. Veneziano[39], M. Vesterinen[11], J.V. Viana Barbosa[38], B. Viaud[7], D. Vieira[2], M. Vieites Diaz[37], X. Vilasis-Cardona[36,p], A. Vollhardt[40], D. Volyanskyy[10], D. Voong[46], A. Vorobyev[30], V. Vorobyev[34], C. Voß[63], J.A. de Vries[41], R. Waldi[63], C. Wallace[48], R. Wallace[12], J. Walsh[23], S. Wandernoth[11], J. Wang[59], D.R. Ward[47], N.K. Watson[45], D. Websdale[53], A. Weiden[40], M. Whitehead[48], D. Wiedner[11], G. Wilkinson[55,38], M. Wilkinson[59], M. Williams[38], M.P. Williams[45], M. Williams[56], H.W. Wilschut[67], F.F. Wilson[49], J. Wimberley[58], J. Wishahi[9], W. Wislicki[28], M. Witek[26], G. Wormser[7], S.A. Wotton[47], S. Wright[47], K. Wyllie[38], Y. Xie[61], Z. Xu[39], Z. Yang[3], X. Yuan[34], O. Yushchenko[35], M. Zangoli[14], M. Zavertyaev[10,b], L. Zhang[3], Y. Zhang[3], A. Zhelezov[11], A. Zhokhov[31], L. Zhong[3].

[1] *Centro Brasileiro de Pesquisas Físicas (CBPF), Rio de Janeiro, Brazil*
[2] *Universidade Federal do Rio de Janeiro (UFRJ), Rio de Janeiro, Brazil*
[3] *Center for High Energy Physics, Tsinghua University, Beijing, China*
[4] *LAPP, Université Savoie Mont-Blanc, CNRS/IN2P3, Annecy-Le-Vieux, France*
[5] *Clermont Université, Université Blaise Pascal, CNRS/IN2P3, LPC, Clermont-Ferrand, France*
[6] *CPPM, Aix-Marseille Université, CNRS/IN2P3, Marseille, France*
[7] *LAL, Université Paris-Sud, CNRS/IN2P3, Orsay, France*
[8] *LPNHE, Université Pierre et Marie Curie, Université Paris Diderot, CNRS/IN2P3, Paris, France*
[9] *Fakultät Physik, Technische Universität Dortmund, Dortmund, Germany*
[10] *Max-Planck-Institut für Kernphysik (MPIK), Heidelberg, Germany*
[11] *Physikalisches Institut, Ruprecht-Karls-Universität Heidelberg, Heidelberg, Germany*
[12] *School of Physics, University College Dublin, Dublin, Ireland*
[13] *Sezione INFN di Bari, Bari, Italy*
[14] *Sezione INFN di Bologna, Bologna, Italy*
[15] *Sezione INFN di Cagliari, Cagliari, Italy*
[16] *Sezione INFN di Ferrara, Ferrara, Italy*
[17] *Sezione INFN di Firenze, Firenze, Italy*
[18] *Laboratori Nazionali dell'INFN di Frascati, Frascati, Italy*
[19] *Sezione INFN di Genova, Genova, Italy*
[20] *Sezione INFN di Milano Bicocca, Milano, Italy*
[21] *Sezione INFN di Milano, Milano, Italy*
[22] *Sezione INFN di Padova, Padova, Italy*
[23] *Sezione INFN di Pisa, Pisa, Italy*
[24] *Sezione INFN di Roma Tor Vergata, Roma, Italy*
[25] *Sezione INFN di Roma La Sapienza, Roma, Italy*
[26] *Henryk Niewodniczanski Institute of Nuclear Physics Polish Academy of Sciences, Kraków, Poland*
[27] *AGH - University of Science and Technology, Faculty of Physics and Applied Computer Science, Kraków, Poland*
[28] *National Center for Nuclear Research (NCBJ), Warsaw, Poland*
[29] *Horia Hulubei National Institute of Physics and Nuclear Engineering, Bucharest-Magurele, Romania*
[30] *Petersburg Nuclear Physics Institute (PNPI), Gatchina, Russia*

JHEP06(2015)131

[31] Institute of Theoretical and Experimental Physics (ITEP), Moscow, Russia
[32] Institute of Nuclear Physics, Moscow State University (SINP MSU), Moscow, Russia
[33] Institute for Nuclear Research of the Russian Academy of Sciences (INR RAN), Moscow, Russia
[34] Budker Institute of Nuclear Physics (SB RAS) and Novosibirsk State University, Novosibirsk, Russia
[35] Institute for High Energy Physics (IHEP), Protvino, Russia
[36] Universitat de Barcelona, Barcelona, Spain
[37] Universidad de Santiago de Compostela, Santiago de Compostela, Spain
[38] European Organization for Nuclear Research (CERN), Geneva, Switzerland
[39] Ecole Polytechnique Fédérale de Lausanne (EPFL), Lausanne, Switzerland
[40] Physik-Institut, Universität Zürich, Zürich, Switzerland
[41] Nikhef National Institute for Subatomic Physics, Amsterdam, The Netherlands
[42] Nikhef National Institute for Subatomic Physics and VU University Amsterdam, Amsterdam, The Netherlands
[43] NSC Kharkiv Institute of Physics and Technology (NSC KIPT), Kharkiv, Ukraine
[44] Institute for Nuclear Research of the National Academy of Sciences (KINR), Kyiv, Ukraine
[45] University of Birmingham, Birmingham, United Kingdom
[46] H.H. Wills Physics Laboratory, University of Bristol, Bristol, United Kingdom
[47] Cavendish Laboratory, University of Cambridge, Cambridge, United Kingdom
[48] Department of Physics, University of Warwick, Coventry, United Kingdom
[49] STFC Rutherford Appleton Laboratory, Didcot, United Kingdom
[50] School of Physics and Astronomy, University of Edinburgh, Edinburgh, United Kingdom
[51] School of Physics and Astronomy, University of Glasgow, Glasgow, United Kingdom
[52] Oliver Lodge Laboratory, University of Liverpool, Liverpool, United Kingdom
[53] Imperial College London, London, United Kingdom
[54] School of Physics and Astronomy, University of Manchester, Manchester, United Kingdom
[55] Department of Physics, University of Oxford, Oxford, United Kingdom
[56] Massachusetts Institute of Technology, Cambridge, MA, United States
[57] University of Cincinnati, Cincinnati, OH, United States
[58] University of Maryland, College Park, MD, United States
[59] Syracuse University, Syracuse, NY, United States
[60] Pontifícia Universidade Católica do Rio de Janeiro (PUC-Rio), Rio de Janeiro, Brazil, associated to [2]
[61] Institute of Particle Physics, Central China Normal University, Wuhan, Hubei, China, associated to [3]
[62] Departamento de Fisica , Universidad Nacional de Colombia, Bogota, Colombia, associated to [8]
[63] Institut für Physik, Universität Rostock, Rostock, Germany, associated to [11]
[64] National Research Centre Kurchatov Institute, Moscow, Russia, associated to [31]
[65] Yandex School of Data Analysis, Moscow, Russia, associated to [31]
[66] Instituto de Fisica Corpuscular (IFIC), Universitat de Valencia-CSIC, Valencia, Spain, associated to [36]
[67] Van Swinderen Institute, University of Groningen, Groningen, The Netherlands, associated to [41]

[a] Universidade Federal do Triângulo Mineiro (UFTM), Uberaba-MG, Brazil
[b] P.N. Lebedev Physical Institute, Russian Academy of Science (LPI RAS), Moscow, Russia
[c] Università di Bari, Bari, Italy
[d] Università di Bologna, Bologna, Italy
[e] Università di Cagliari, Cagliari, Italy
[f] Università di Ferrara, Ferrara, Italy
[g] Università di Firenze, Firenze, Italy
[h] Università di Urbino, Urbino, Italy
[i] Università di Modena e Reggio Emilia, Modena, Italy
[j] Università di Genova, Genova, Italy
[k] Università di Milano Bicocca, Milano, Italy
[l] Università di Roma Tor Vergata, Roma, Italy

JHEP06(2015)131

[m] *Università di Roma La Sapienza, Roma, Italy*
[n] *Università della Basilicata, Potenza, Italy*
[o] *AGH - University of Science and Technology, Faculty of Computer Science, Electronics and Telecommunications, Kraków, Poland*
[p] *LIFAELS, La Salle, Universitat Ramon Llull, Barcelona, Spain*
[q] *Hanoi University of Science, Hanoi, Viet Nam*
[r] *Università di Padova, Padova, Italy*
[s] *Università di Pisa, Pisa, Italy*
[t] *Scuola Normale Superiore, Pisa, Italy*
[u] *Università degli Studi di Milano, Milano, Italy*
[v] *Politecnico di Milano, Milano, Italy*

JHEP06(2015)131